

Spatial-Confinement Induced Electroreduction of CO and CO₂ to Diols on Densely-Arrayed Cu Nanopyramids

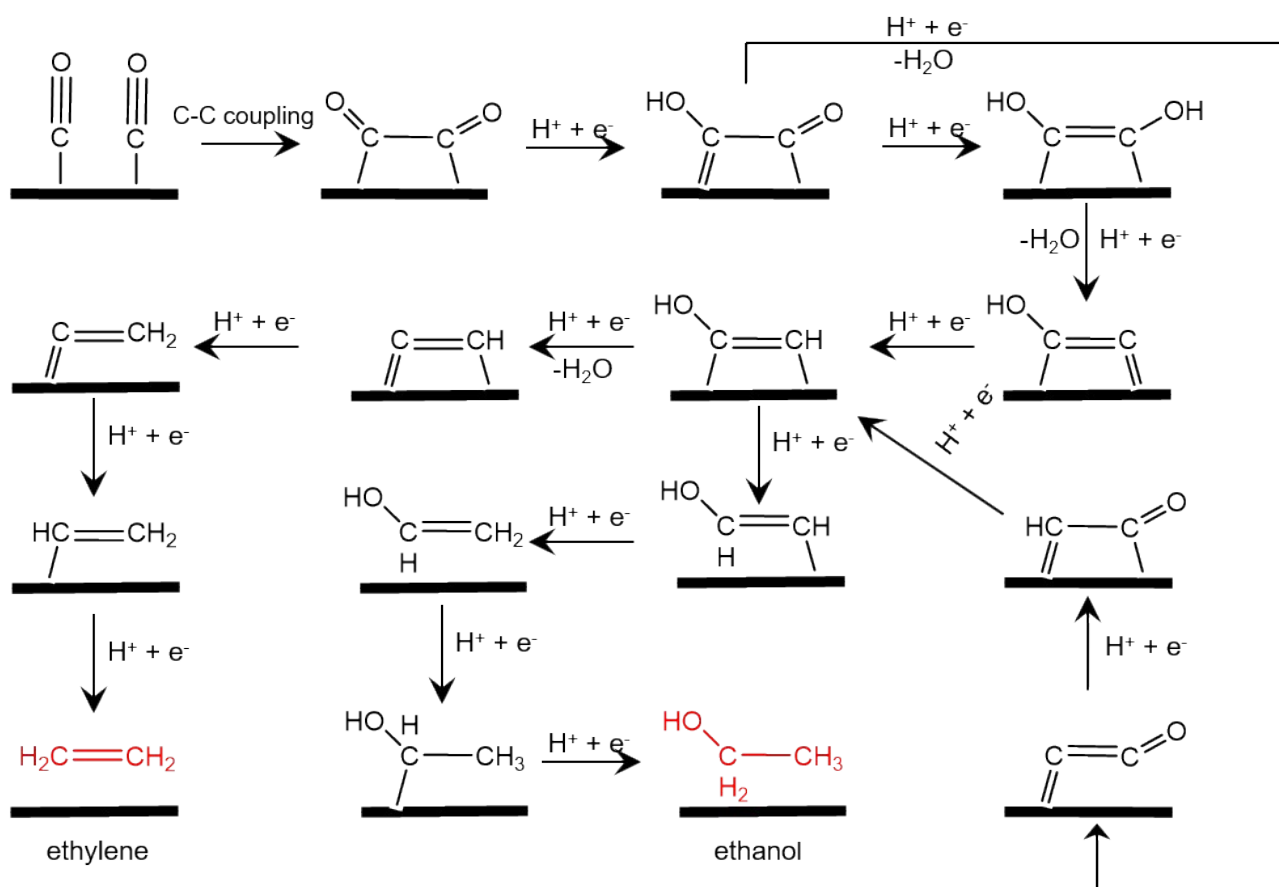
Ling Chen, Cheng Tang, Kenneth Davey, Yao Zheng, Yan Jiao* and Shi-Zhang Qiao*

School of Chemical Engineering and Advanced Materials, The University of Adelaide, South Australia 5005, Australia

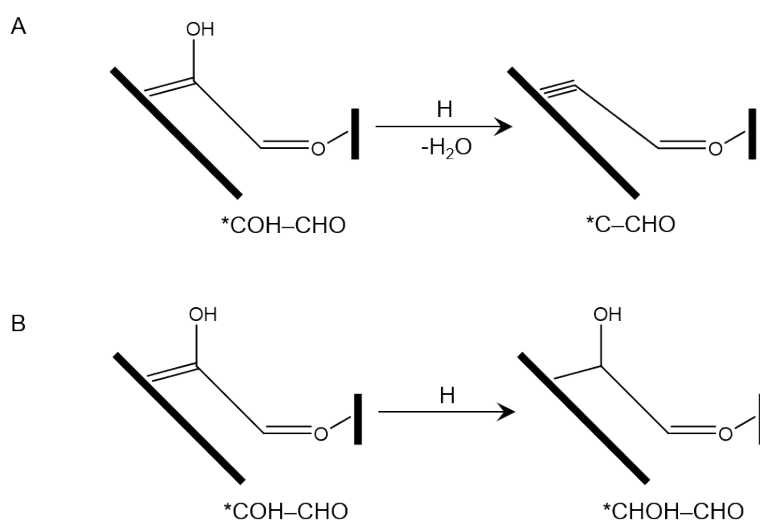
Corresponding author: * yan.jiao@adelaide.edu.au; s.qiao@adelaide.edu.au

This file includes:

- **Schemes S1-S2**
- **Figures S1-S20**
- **Supplementary Notes 1-4**
- **Tables S1-S15**
- **Supplementary References**



Scheme S1. Conventional *COH-COH and *C-CO pathways on Cu (100) following adsorption of two CO intermediates.¹⁻³



Scheme S2. Further hydrogenation step for *COH-CHO on Cu-DAN to: (A) *C-CHO, and; (B) *CHOH-CHO.

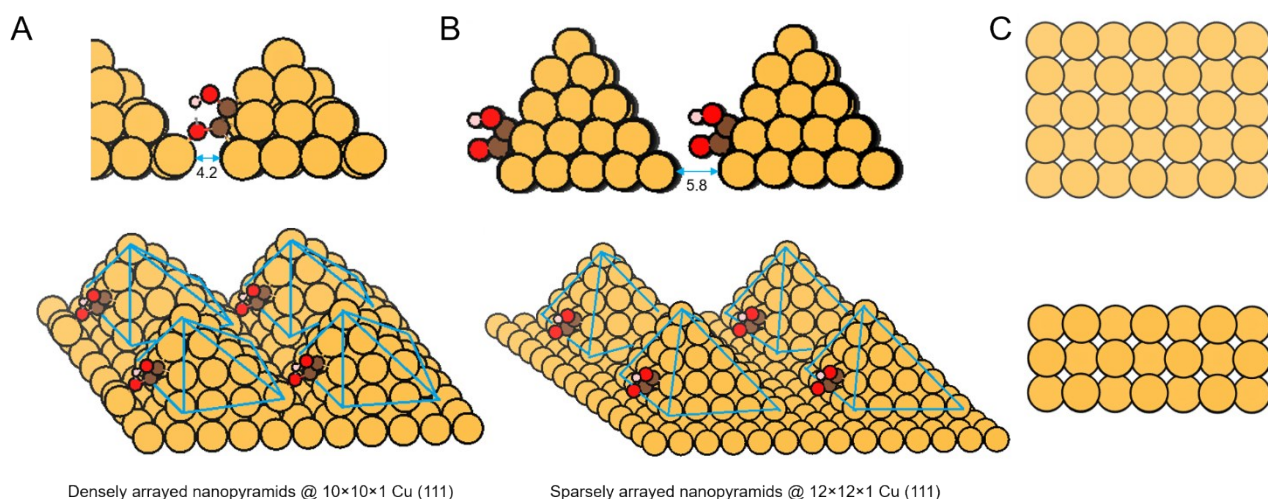


Fig. S1. Close-up (top panel) and overall (bottom panel) view of $^*COH-CO$ adsorption on: (A) densely-arrayed Cu nanopyramids, (B) sparsely-arrayed Cu nanopyramids, and top and side view of (C) planar Cu (100). The [111] diamond nanopyramid was built based on a $10 \times 10 \times 1$ Cu surface with 4.2 \AA distance between two nanopyramids to represent the dense-array, and on a $12 \times 12 \times 1$ Cu surface to represent the sparse-array with 5.8 \AA distance. Distance in figure is \AA . Color code: Cu, orange; C, brown; O, red; H, pink. Solid-blue lines serve as a visual guide for the pyramid.

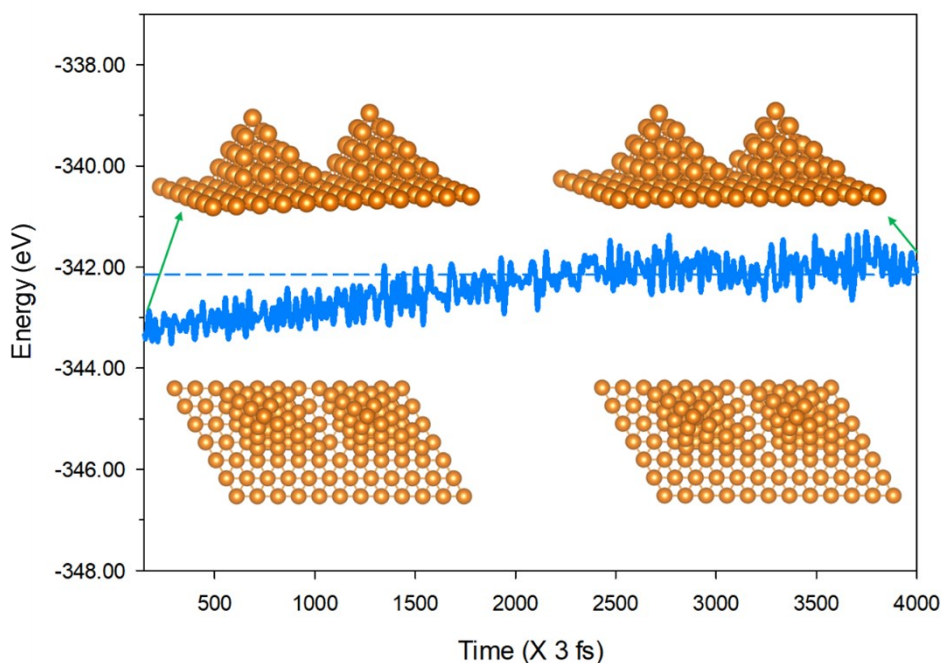


Fig. S2. *Ab initio* molecular dynamics (AIMD) simulated energy evolution for Cu-DAN at 300 K. Insets show the top and side views of the snapshots of atomic configurations at 0 and 12 ps. The blue dashed-line denotes equilibrium position.

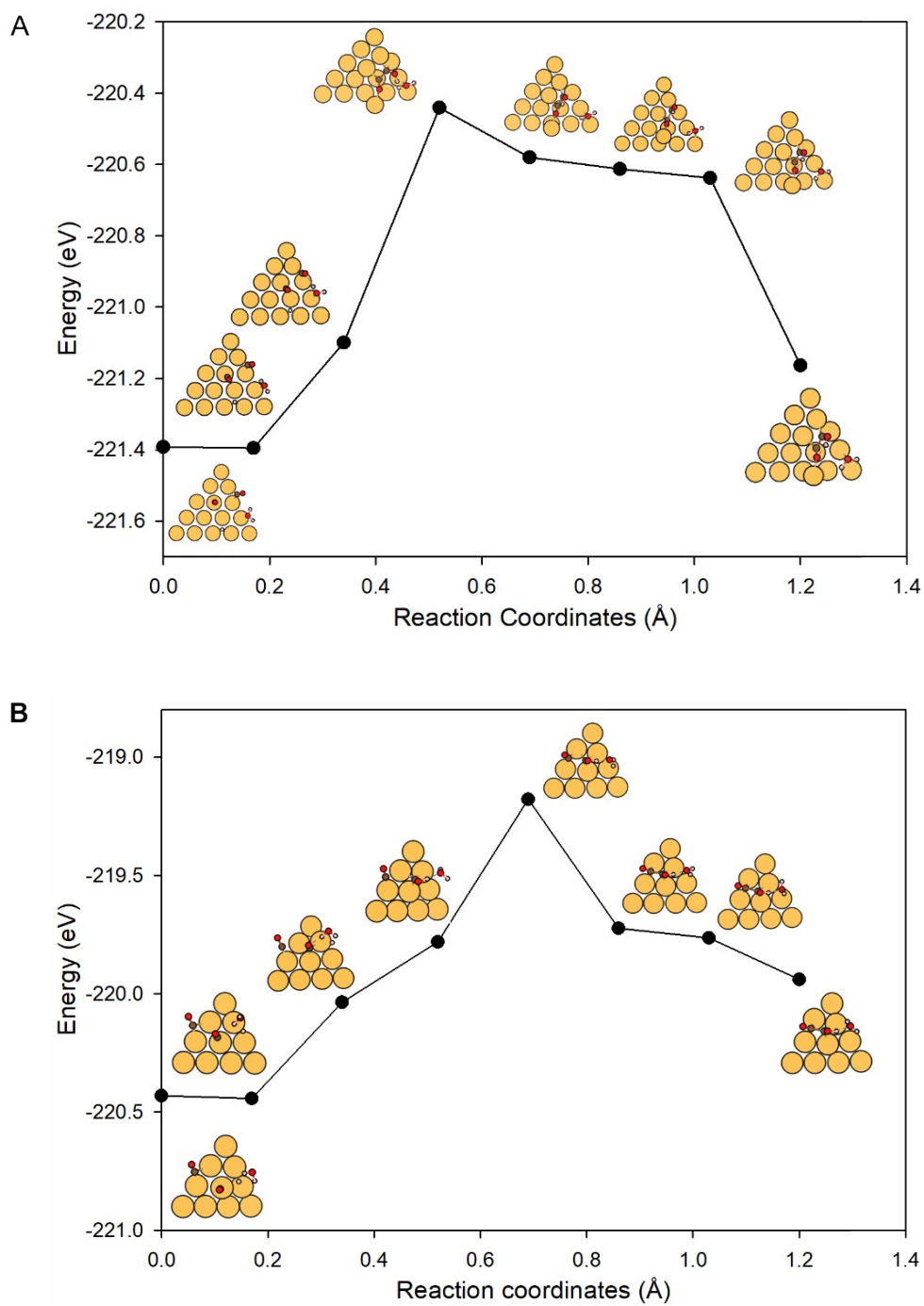


Fig. S3. Minimum energy path (MEP) involved in $*CO + *CO + H^+ + e^- \rightarrow *COH-CO$ via H-shuttling on (A) Cu-DAN, and (B) Cu-SAN. Color code: Cu, orange; C, brown; O, red; H, pink. Energy barrier in (A) is $\Delta G^\ddagger(U^0) = 1.07$ eV and in (B), $\Delta G^\ddagger(U^0) = 1.50$ eV.

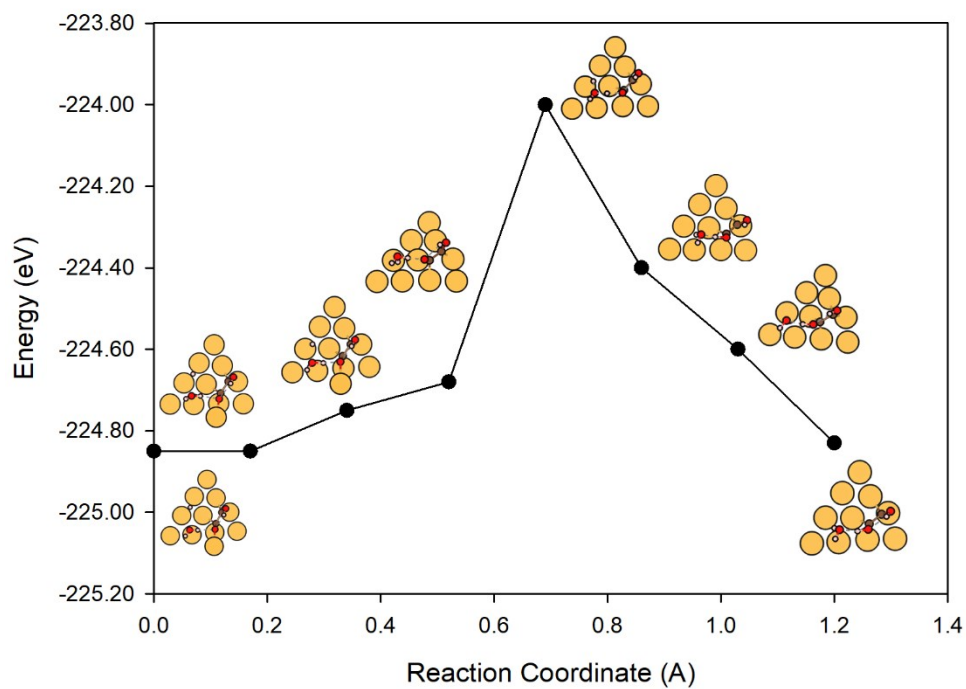


Fig. S4. MEP involved in $*\text{COH-CO} + \text{H}^+ + \text{e}^- \rightarrow *\text{COH-COH}$ on Cu-DAN via H-shuttling. Color code: Cu, orange; C, brown; O, red; H, pink. Energy barrier is $\Delta G^\ddagger(\text{U}^0) = 0.76$ eV.

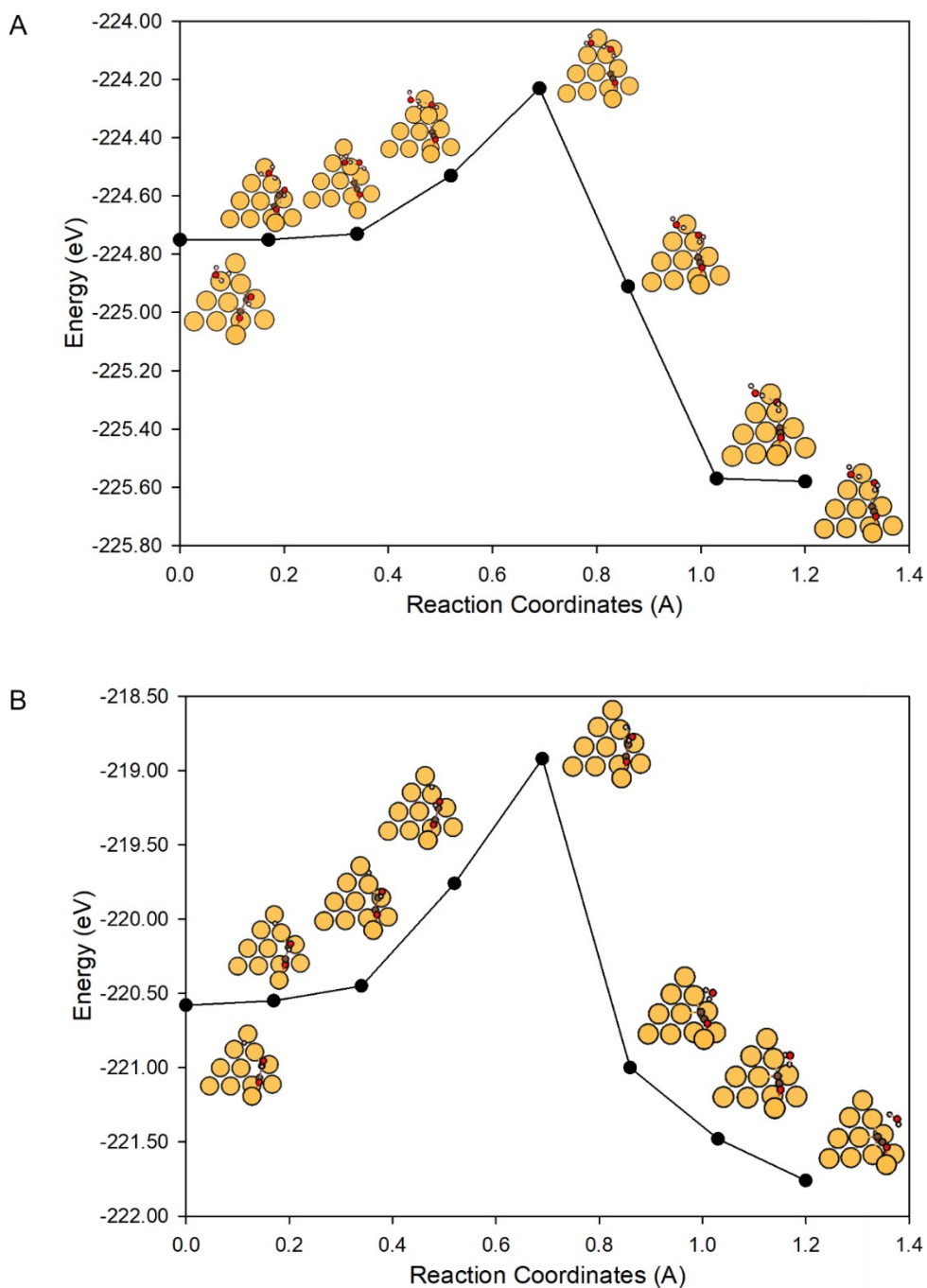


Fig. S5. MEP involved in $*\text{COH-CO} + \text{H}^+ + \text{e}^- \rightarrow * \text{C-CO} + \text{H}_2\text{O}$ on Cu-DAN via (A) H-shuttling and (B) surface *H transfer. Color code: Cu, orange; C, brown; O, red; H, pink. Energy barrier value in (A) is $\Delta G^\ddagger(U^0) = 0.72$ eV and in (B), $\Delta G^\ddagger(U^0) = 1.66$ eV

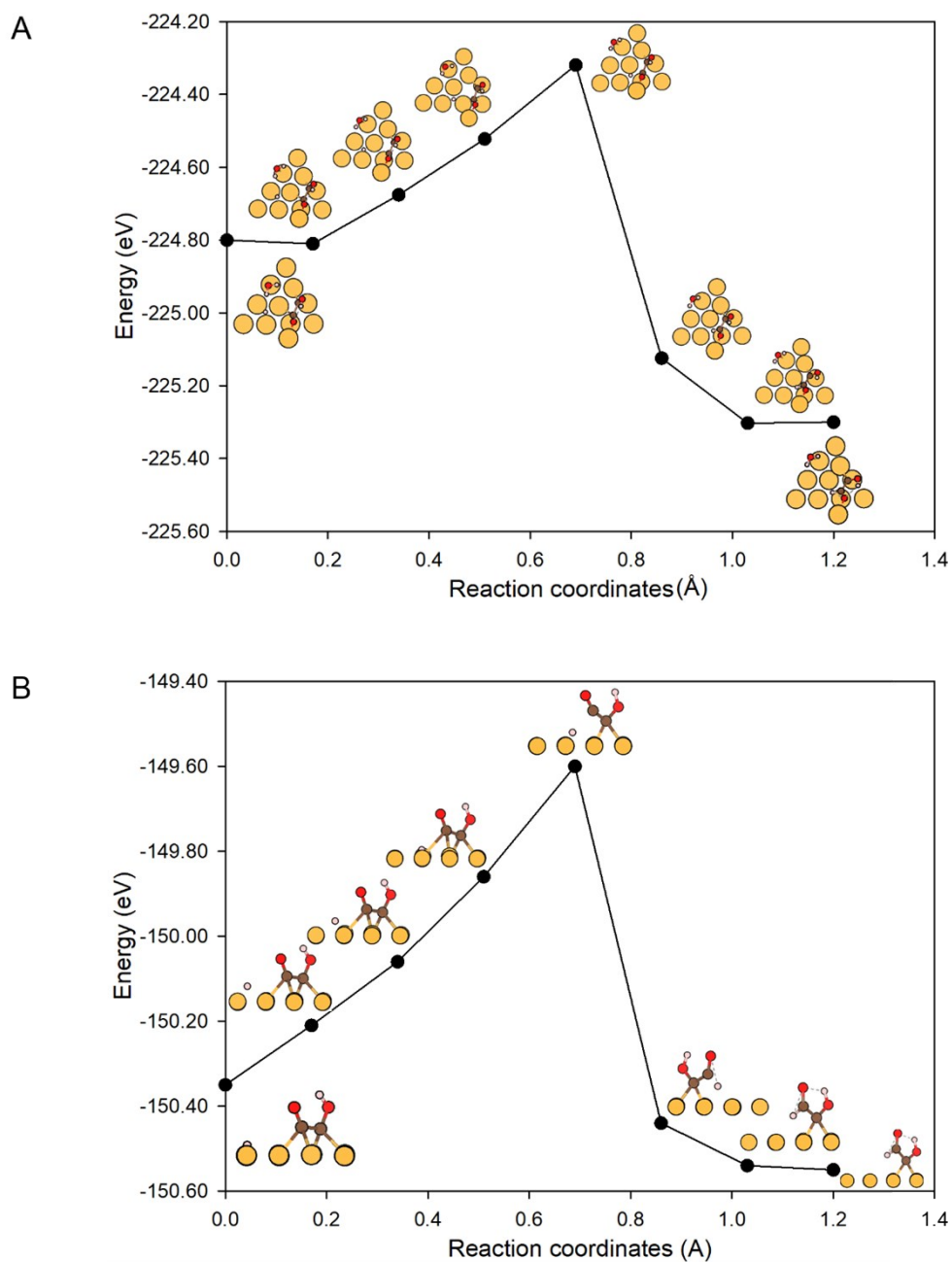


Fig. S6. MEP involved in $*\text{COH-CO} + \text{H}^+ + \text{e}^- \rightarrow *\text{COH-CHO}$ via surface $*\text{H}$ transfer on (A) Cu-DAN and (B) planar Cu (100). Color code: Cu, orange; C, brown; O, red; H, pink. Energy barrier in (A) is $\Delta G^\ddagger(U^0) = 0.41$ eV, in (B) $\Delta G^\ddagger(U^0) = 0.69$ eV.

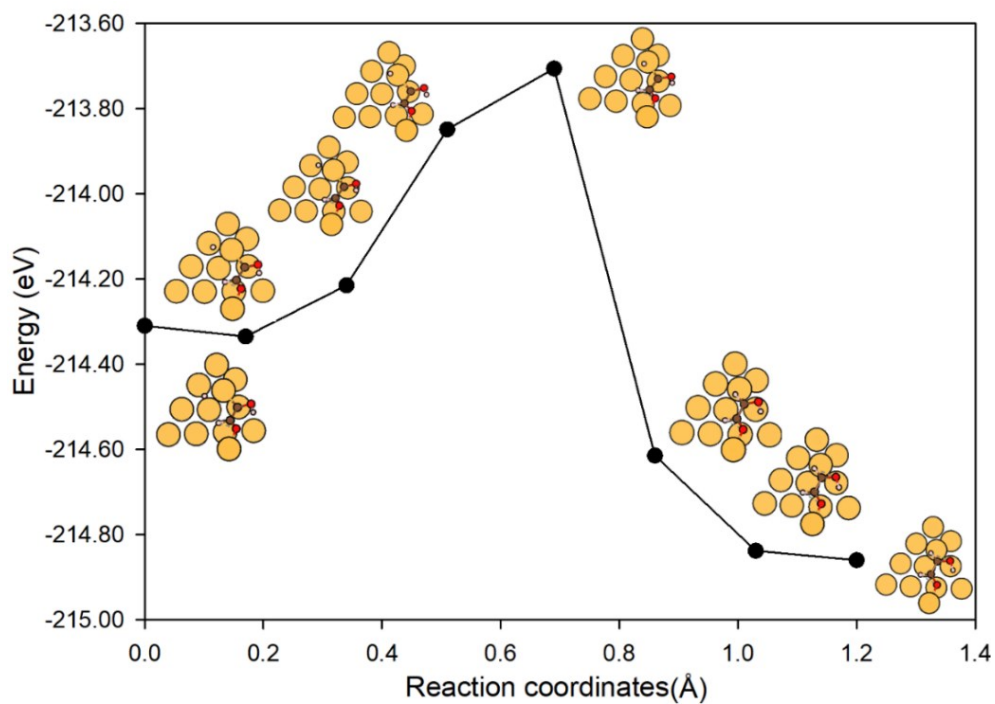


Fig. S7. MEP involved in $*\text{COH-CHO} + \text{H}^+ + \text{e}^- \rightarrow *\text{CHOH-CHO}$ via surface $*\text{H}$ transfer on Cu-DAN. Color code: Cu, orange; C, brown; O, red; H, pink. Energy barrier value is $\Delta G^\ddagger(U^0) = 0.52$ eV.

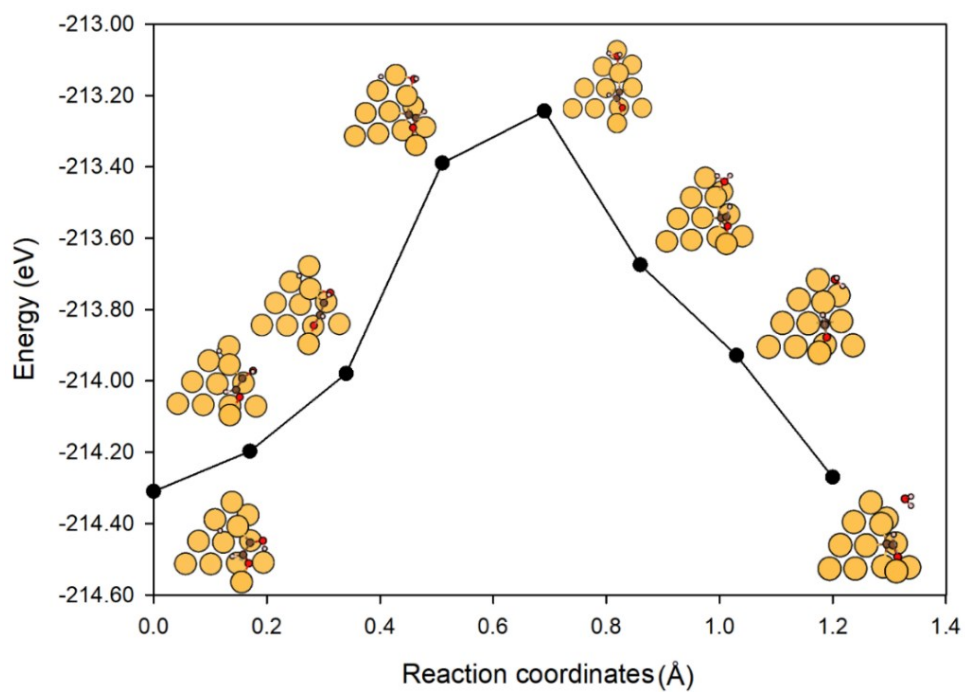


Fig. S8. MEP involved in $*\text{COH-CHO} + \text{H}^+ + \text{e}^- \rightarrow * \text{C-CHO} + \text{H}_2\text{O}$ on Cu-DAN via surface $*\text{H}$ transfer. Color code: Cu, orange; C, brown; O, red; H, pink. Energy barrier value is $\Delta G^\ddagger(\text{U}^0) = 1.02$ eV.

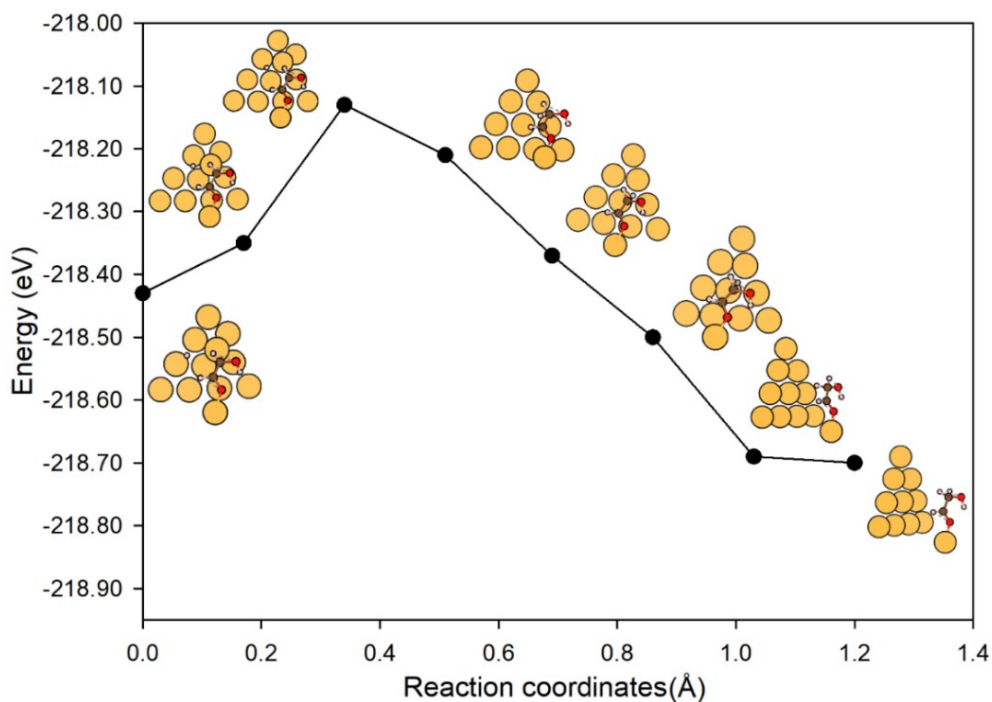


Fig. S9. MEP involved in $*\text{CHOH-CHO} + \text{H}^+ + \text{e}^- \rightarrow * \text{CH}_2\text{OH-CHO}$ on Cu-DAN via surface $*\text{H}$ transfer. Color code: Cu, orange; C, brown; O, red; H, pink. Energy barrier value is $\Delta G^\ddagger(\text{U}^0) = 0.25$ eV.

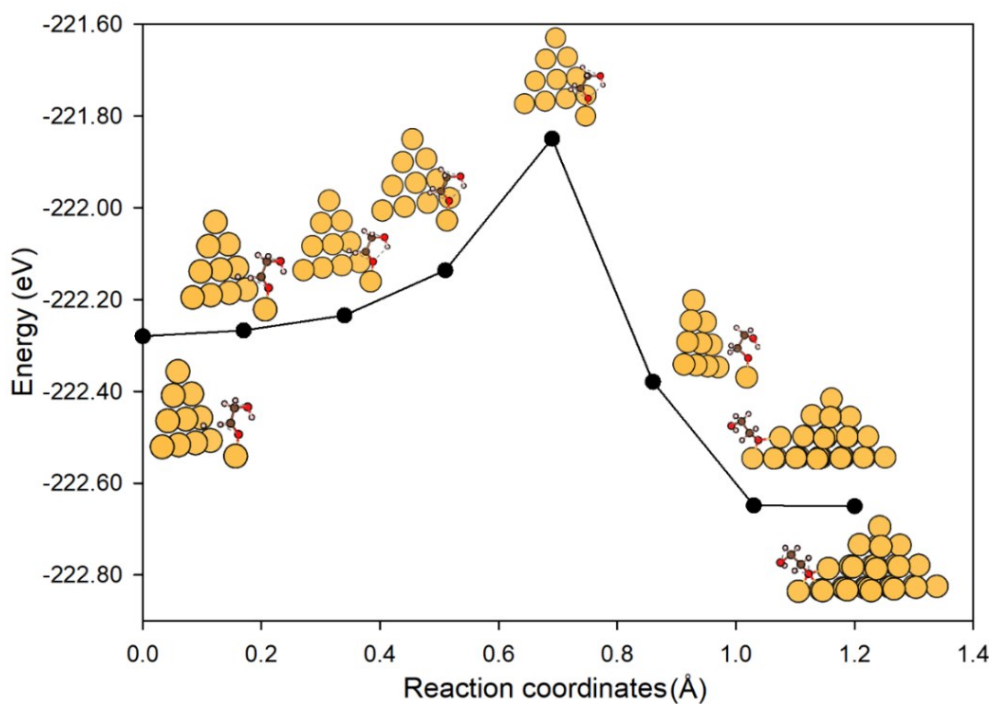


Fig. S10. MEP involved in $*\text{CH}_2\text{OH}-\text{CHO} + \text{H}^+ + \text{e}^- \rightarrow *\text{CH}_2\text{OH}-\text{CH}_2\text{O}$ on Cu-DAN via surface $*\text{H}$ transfer. Color code: Cu, orange; C, brown; O, red; H, pink. Energy barrier value is $\Delta G^\ddagger(\text{U}^0) = 0.39$ eV.

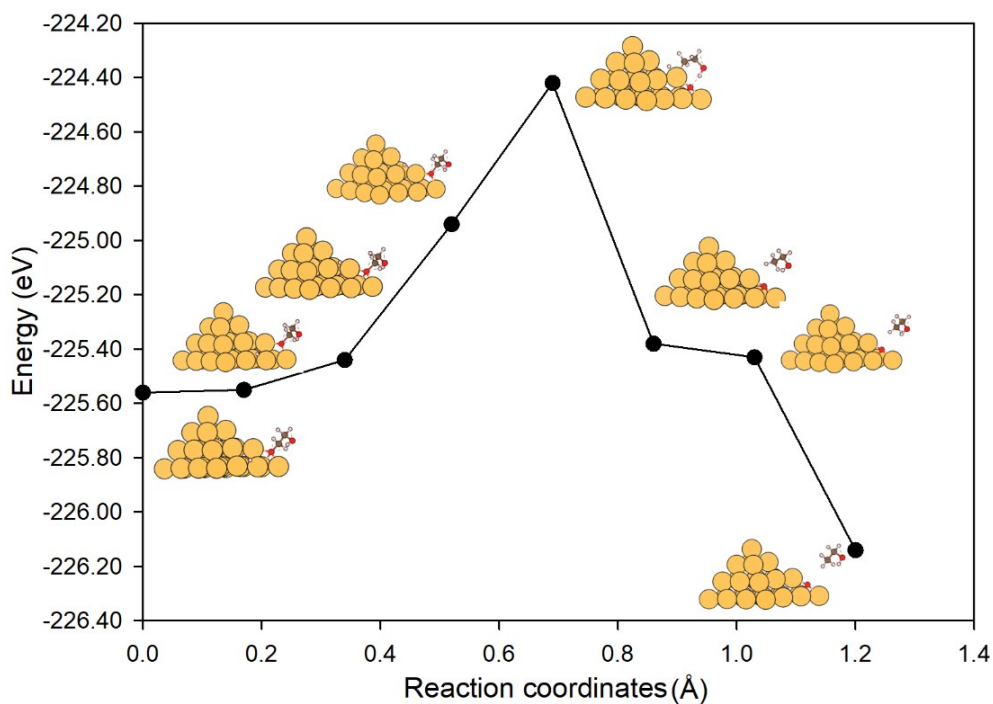


Fig. S11. MEP involved in $*\text{CH}_2\text{OH}-\text{CH}_2\text{O} + \text{H}^+ + \text{e}^- \rightarrow \text{CH}_2\text{OH}-\text{CH}_3 + *\text{O}$ on Cu-DAN via surface $*\text{H}$ transfer. Color code: Cu, orange; C, brown; O, red; H, pink. Energy barrier value is $\Delta G^\ddagger(\text{U}^0) = 0.98$ eV.

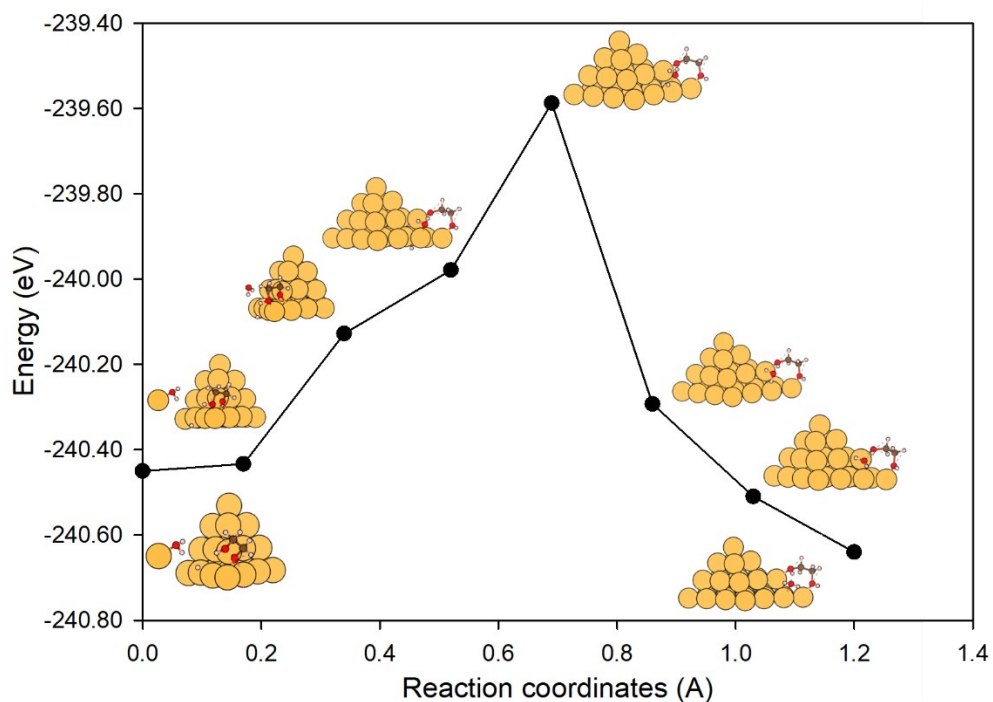


Fig. S12. MEP involved in $*\text{CH}_2\text{OH}-\text{CH}_2\text{O} + \text{H}^+ + \text{e}^- \rightarrow *\text{CH}_2\text{OH}-\text{CH}_2\text{OH}$ on Cu-DAN via H-shuttling. Color code: Cu, orange; C, brown; O, red; H, pink. Energy barrier value is $\Delta G^\ddagger(\text{U}^0) = 0.73$ eV.

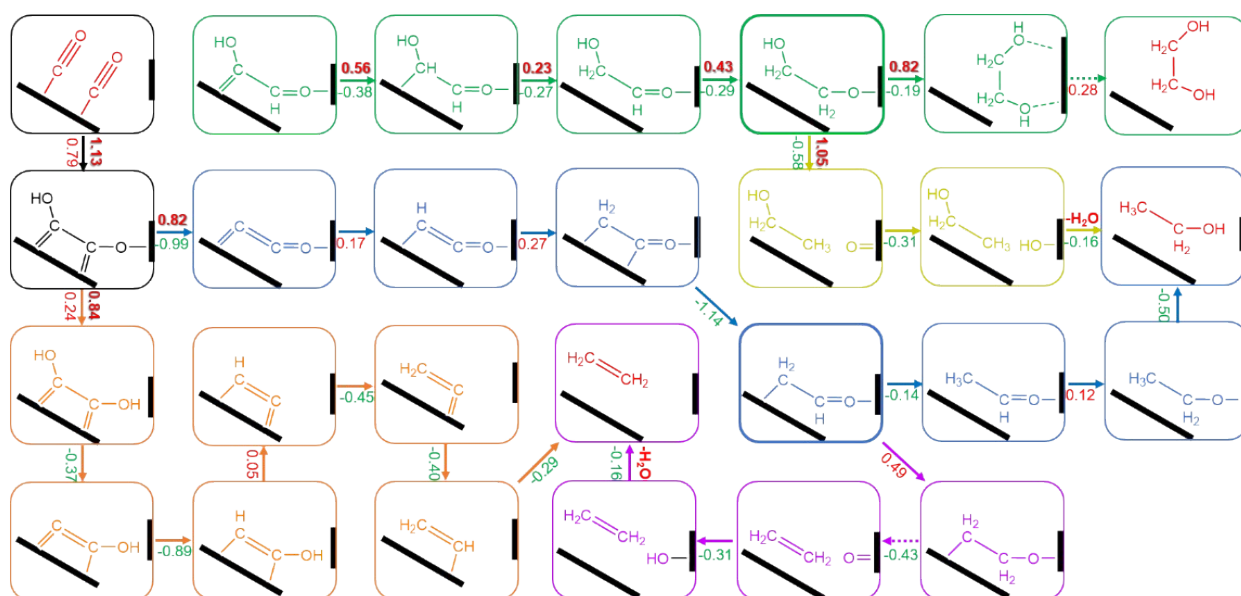


Fig. S13 Chemical structure of reaction intermediates in different pathways on Cu-DAN. Pathways toward C_2 products (ethylene, ethanol and ethylene glycol) beyond 2 $*CO$ are shown as colored-branches: orange, $*COH-COH$ pathway toward C_2H_4 ; blue, $*C-CO$ pathway toward C_2H_5OH ; purple, $*C-CO$ pathway bifurcating to C_2H_4 ; green, $*COH-CHO$ pathway toward $C_2H_6O_2$, and; brown, $*COH-CHO$ pathway bifurcating to C_2H_5OH . Reaction barrier ΔG^\ddagger values at 0 V vs RHE appear in bolded- and shaded-font. Free energy change ΔG values appear in standard-font. Green and red values denote, respectively, exergonic and endergonic process. The solid-arrow denotes proton-coupled electron transfer ($H^+ + e^-$), and dotted-arrow denotes desorption. The unit of energy is eV.

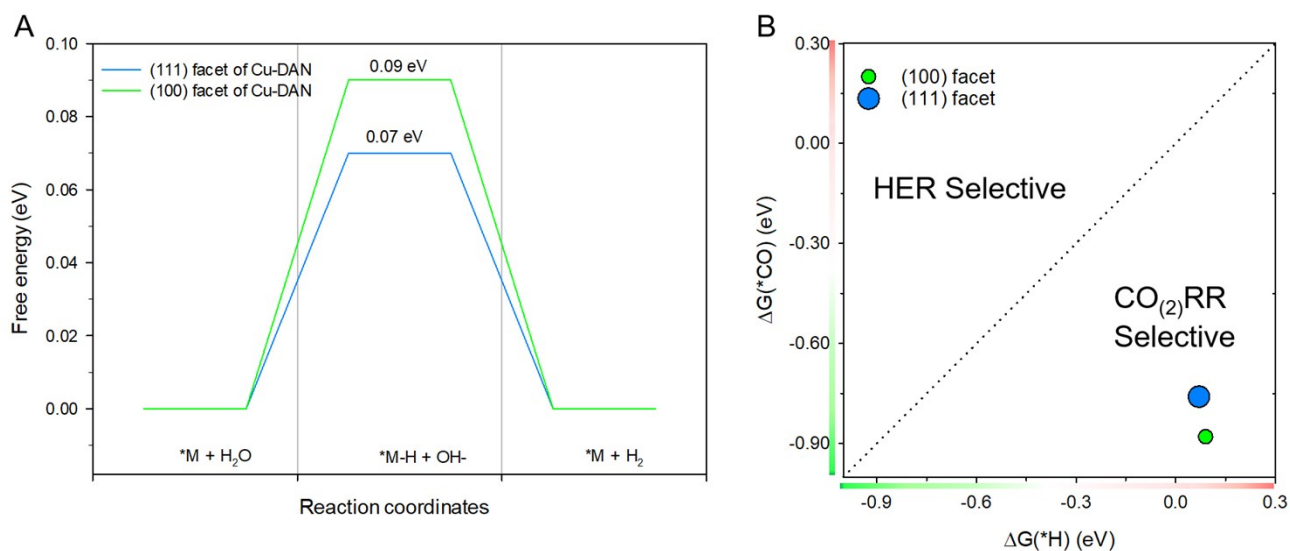


Fig. S14. (A) Free energy diagram for HER on Cu-DAN. (B) Comparison between hydrogen adsorption free energy $\Delta G(*H)$ and carbon monoxide adsorption free energy $\Delta G(*CO)$ on (111) and (100) facets of Cu-DAN.

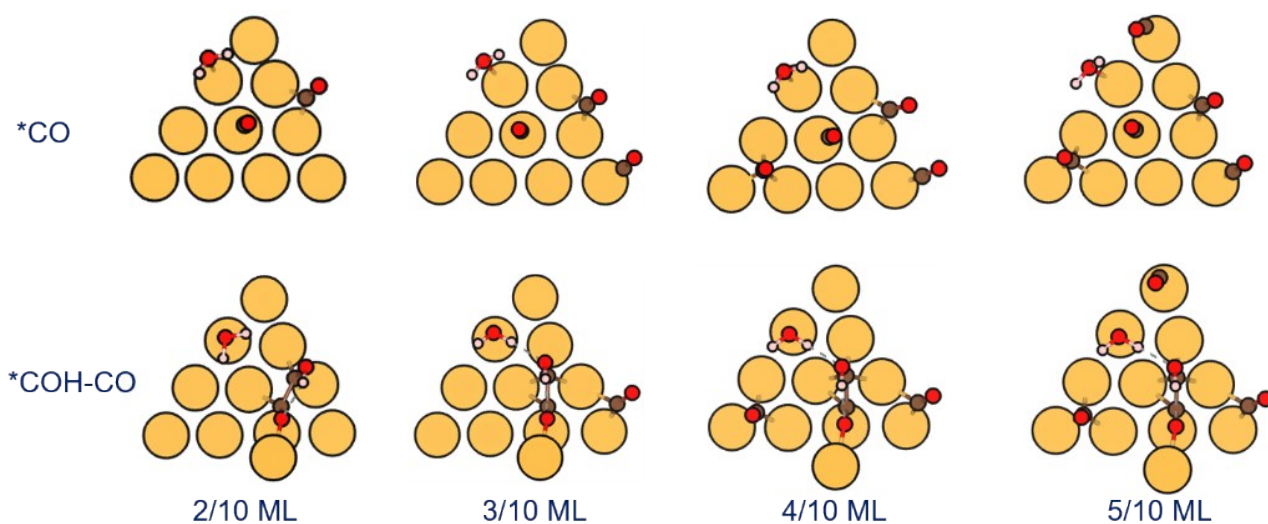


Fig. S15. Atomic structures of *CO and *COH-CO under *CO coverage of 2/10, 3/10, 4/10 and 5/10 ML. Color code: Cu, orange; C, brown; O, red; H, pink.

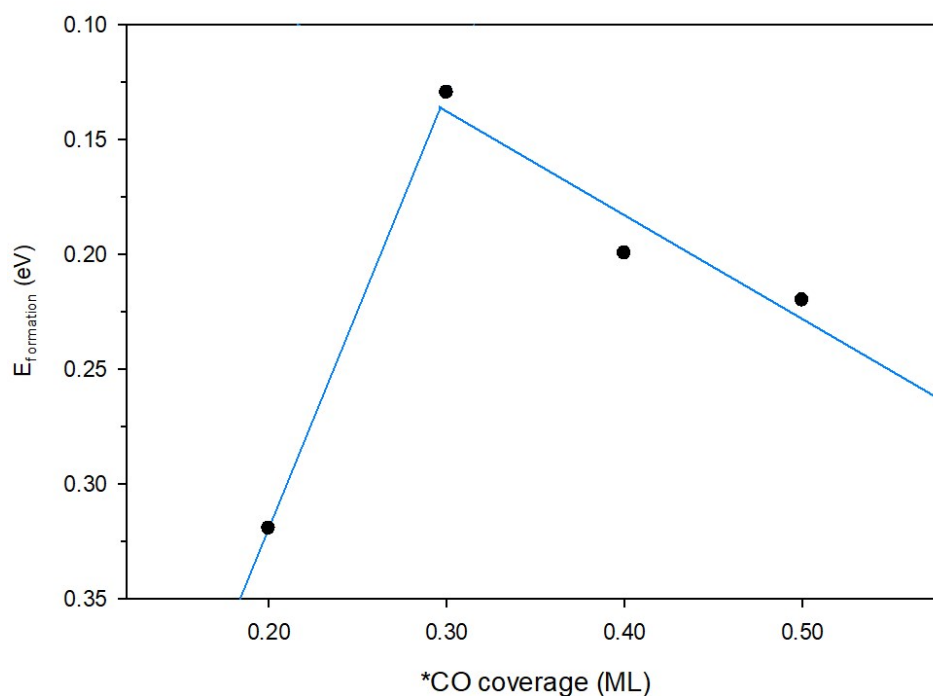


Fig. S16. Volcano-type relationship between *CO coverage and formation energy of *COH-CO .

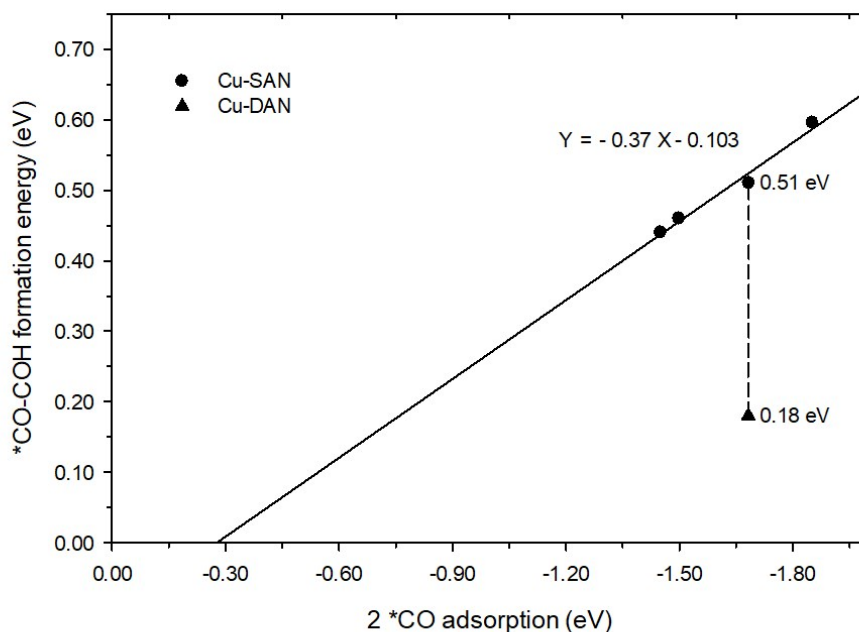


Fig. S17. Linear scaling relations between 2*CO adsorption and *COH–CO formation free energies on Cu-SAN and Cu-DAN.

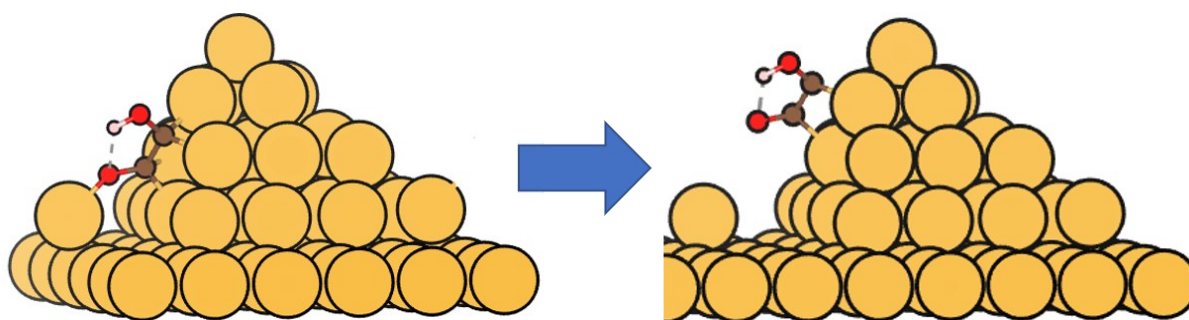


Fig. S18. Computation of Cu–O bond strength. To compute the strength of the bond between β O and Cu of the adjacent nanopyramid, we moved the *COH–CO along the nanopyramid surface until the Cu–O bond was completely broken. The energy difference between the translated structure with original is 2.63 eV (253.76 kJ mol⁻¹), and reflects the Cu–O bond strength. All atoms were fixed to compute the single-point energy of the structure.

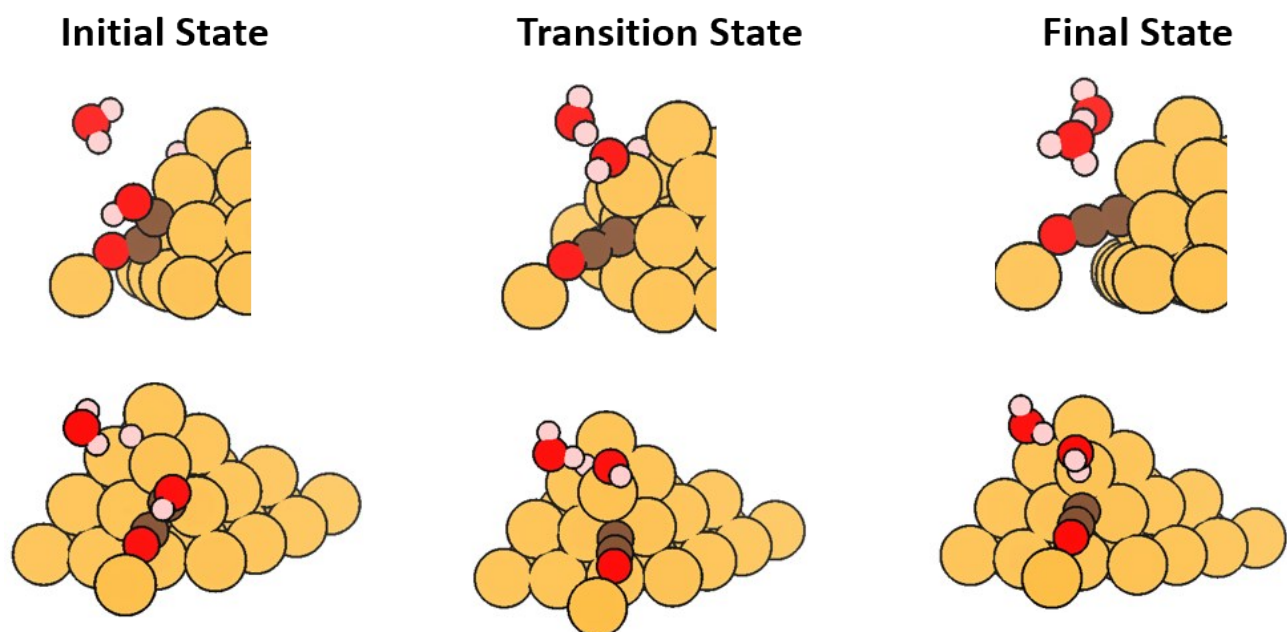


Fig. S19. Side and front view of optimized structures of, respectively, the initial, transition and final states involved in $^*\text{COH-CO}$ reduction to $^*\text{C-CO}$ on Cu-DAN. Color code: Cu, orange; C, brown; O, red; H, pink.

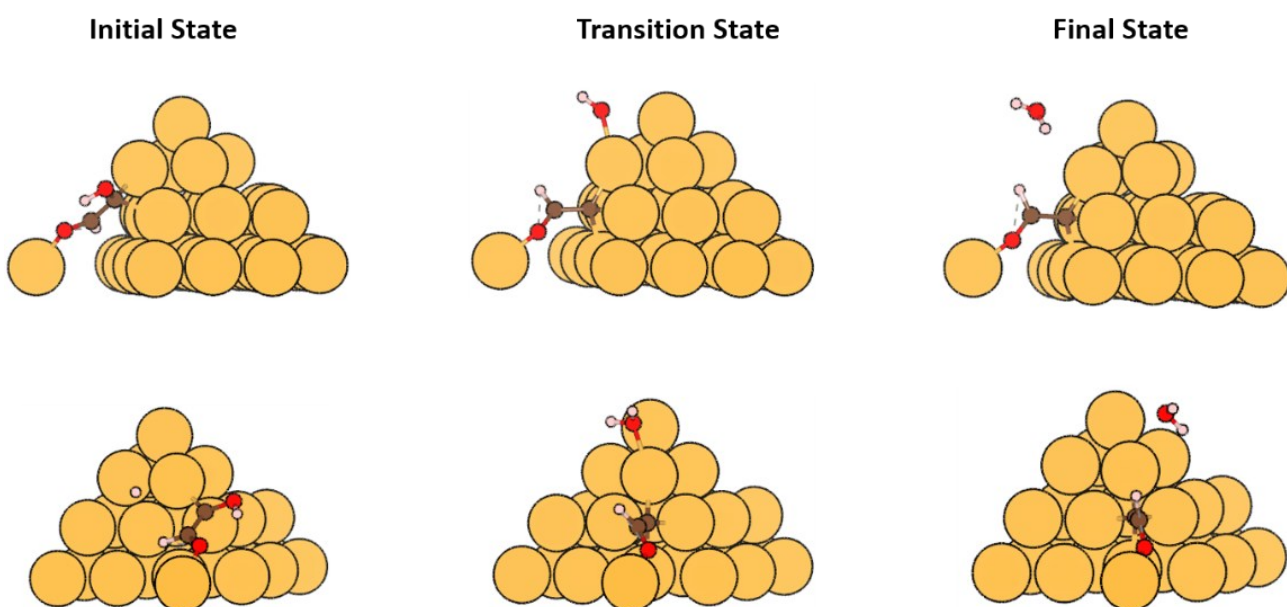


Fig. S20. Side and front view of optimized structures of, respectively, the initial, transition and final states involved in $^*\text{COH-CHO}$ reduction to $^*\text{C-CHO}$ on Cu-DAN ($^*\text{COH-CHO} + \text{H}^+ + \text{e}^- \rightarrow ^*\text{C-CHO} + \text{H}_2\text{O}$). Color code: Cu, orange; C, brown; O, red; H, pink.

Supplementary Note 1

Stability of Cu-DAN

Stability is a prerequisite for electrocatalytic materials. This is closely related to the experimental feasibility and catalytic activity for long-term use.

The dissolution potential (U_{diss}) of the surface atoms on nanopyramid, which assess the dissolution-resistance of one surface atom from the nanopyramid into water under an applied potential,⁸ is calculated as:

$$U_{\text{diss}} = U_{\text{diss}(\text{Cu})}^0 - E_f / ne$$

where $U_{\text{diss}(\text{Cu})}^0$ and n denote standard reduction potential of Cu and the number of electrons transferred during dissolution. The values are 0.34 V and 2, respectively.

E_f , the formation energy of one surface Cu atom, is defined as:

$$E_f = E_{\text{nanopyramid}} - E_{\text{less}} - E_{\text{Cu}}$$

where $E_{\text{nanopyramid}}$ is the total energy, E_{less} is the energy of nanopyramid without one surface Cu atom and E_{Cu} is the energy of isolated Cu atom.

The calculated positive U_{diss} of 1.72 V shows that the surface Cu atoms will be stable under electrochemical environments.

In addition, we carried out *ab initio* molecular dynamics (AIMD) simulations to explore the thermodynamic stability of the surface atoms of the Cu-DAN at 300K, as shown in Figure S2. We found that the thermal oscillations of surface Cu atoms occur near the equilibrium position following relaxation for 6 ps, and that the structure showed no significant structural distortion. This finding confirms thermodynamic stability of Cu-DAN.

Supplementary Note 2

Hydrogen evolution reaction (HER) on Cu-DAN

We used DFT computations to identify that the most stable *H adsorption sites, with minimum adsorption energy on Cu nanopyramids, is the 4-fold hollow site for (100) facets, and HCP hollow site for (111) facets, respectively. The performance of these active sites for the Volmer step of HER in alkaline condition ($*M + H_2O + e^- \rightarrow *M-H + OH^-$) was investigated using free energy as an indicator. The free energy change of the Volmer step can be computed from:

$$\Delta G_{volmer} = (G_{*M-H} + G_{OH^-}) - (G_{*M} + G_{H_2O} + G_{e^-})$$

where G_{*M} is the free energy of the original pyramidal structure, G_{*M-H} is the free energy of the pyramidal structure with adsorbed *H, G_{H_2O} and G_{H_2} is the free energy of a H_2O molecule and a H_2 molecule. G_{OH^-} is the free energy of a hydroxide ion (OH^-) obtained as, $G_{OH^-} = G_{H_2O} - G_{H_2}/2$.

The computational results are given in Figure S14A, and a comparison with *CO adsorption energy on the same sites is given in Figure S14B that indicates suppression of competing HER on Cu-DAN.

Supplementary Note 3

Effect of *CO coverage on the formation of *COH-CO

The coverage of *CO is expressed in monolayer (ML) units. These are defined as the number of adsorbed *CO molecules (n , $n = 2, 3, 4$ and 5 in this simulation) divided by the total number of atoms on one facet of Cu-DAN (10). The formation energy of intermediate *COH-CO under such *CO coverage then is computed as:

$$E_{\text{formation}} = E_{\text{total}} - (E_{\text{slab}+n*\text{CO}} + E_{\text{H}_2}/2)$$

where E_{total} is the energy of the total system, $E_{\text{slab}+n*\text{CO}}$ is the energy of Cu-CAN with adsorption of n *CO molecules. E_{H_2} is the energy of a hydrogen molecule (-6.76 eV).

We began by constructing the Cu-DAN surface with two *CO adsorbates (*CO coverage = 2/10 ML). To investigate the influence of *CO coverage on the formation of *COH-CO we added more *CO molecules on the surface to gradually increase the *CO coverage from 2/10 to 5/10 ML as is shown in Figure S15. We found volcano-type relationships between *CO coverage and formation energy of *COH-CO (Figure S16). With the increase of *CO coverage, the formation energy of *COH-CO increases first and reaches a peak at 3/10 ML. This is consistent with experimental observations that a higher *CO coverage promotes C-C coupling.

As the *CO coverage increases further, the formation energy of *COH-CO decreases. This is because the steric hindrance of O atom caused by excessive *CO adsorption destabilizes the dimer intermediate *COH-CO.

Supplementary Note 4

***COH–CHO formation on planar Cu (100)**

*COH–CHO is the precursor of glycolaldehyde (CH₂OH–CHO). Two mechanisms have been hypothesized toward its formation on planar Cu surface.¹ These are: 1) *COH–CO + H → *COH–CHO, and; 2) *CHO + *COH → *COH–CHO. On planar Cu (100) surface *COH–COH prevails over *COH–CHO. The reason is discussed in detail.

For the first mechanism Cheng et al.¹ hypothesized a pathway on planar Cu (100) facets in which *COH–CO formation is followed by hydrogenation of βO atoms. This rules out the possibility of hydrogenation of βC to *COH–CHO. We attribute this to the instability of intermediate *COH–CHO. The structures of *COH–CHO and *COH–COH are tautomeric. The former is comparatively unstable because it is vertically adsorbed on surface via a double bond, and because it has a free radical on the C atom. We computed *COH–CHO to be 0.26 eV less stable than *COH–COH on planar Cu (100) surface.

This finding means the bulk of *COH–CHO are spontaneously tautomerized to *COH–COH, despite being formed first. Because *COH–CHO is not a stable molecular compound with a significant concentration on planar Cu (100) surface, the *COH–CHO pathway is blocked. Additionally if the formation of *COH–CHO follows the second mechanism, it is difficult for it to proceed on a planar surface. *COH and *CHO are preferably, respectively, stabilized on Cu (111) and Cu (100) surface.⁴

It is reportedly rare for those two adsorbates to simultaneously attain the kinetically reactable concentration on a homogeneous facet. This is the reason why we record a high-level barrier of 0.72 eV at 0 V vs RHE for *COH–CHO formation on planar Cu (100) surface.

We conclude therefore that on a planar Cu (100) surface *COH–CHO is not favored and the pathway is blocked.

Table S1. Free energy for gas phase species.

<i>Gas Molecule</i>	<i>E</i> (eV)	<i>ZPE</i> (eV)	<i>-TS</i> (eV)	<i>G</i> (eV)
H ₂ (g)	-6.75	0.27	-0.41	-6.89
H ₂ O (g)	-14.22	0.56	-0.67	-14.33
CO (g)	-14.80	0.13	-0.61	-14.70
CO ₂ (g)	-23.01	0.31	-0.66	-23.36
C ₂ H ₄ (g)	-31.97	1.37	-0.55	-31.15
C ₂ H ₅ OH (g)	-46.88	2.13	-0.60	-45.35
(CH ₂ OH) ₂ (g)	-53.31	2.27	-0.65	-51.69

Table S2. Summary of elementary reaction steps, hydrogen transfer model, reaction barriers at various electrode potentials and involved parameter for computation. $\Delta G(0V)$ and $\Delta G^\ddagger(0V)$ are the free energy change and reaction barrier without potential bias, $\Delta G^\ddagger(U^0)$ is the reaction barrier under U^0 . U^0 is the equilibrium potential for the reductive adsorption of one proton in the system, and β' is the reaction symmetry factor, as defined in the manuscript. The two hydrogen models considered were, 1) Langmuir-Hinshelwood (LH) mechanism (i.e. direct transfer of an adsorbed *H), and 2) Eley-Rideal (ER) mechanism (i.e. water molecule shuttles an adsorbed *H). Adding hydrogen to carbon species via LH mechanism always gives lower kinetic barriers, compared with hydrogen transfer via ER mechanism. ER mechanism contributed to a lower kinetic barrier when hydrogen is added to oxygen species.^{5,6} For all steps computed with H-shuttling, one H₂O molecule was included in the computation.

No.	Catalyst	Reaction Steps	Model	$\Delta G(0V)$	$\Delta G^\ddagger(U^0)$	U^0 ^a	β' ^b	$\Delta G^\ddagger(0V)$
1a	Cu-DAN	*CO+*CO+H ⁺ +e ⁻ →*COH-CO	H-shuttling	0.79	1.07	-0.12	0.49	1.13
1b	Cu-SAN		H-shuttling	0.94	1.50	-0.25	0.49	1.63
2	Cu-DAN	*COH-CO+ H ⁺ +e ⁻ →*COH-COH	H-shuttling	0.24	0.76	-0.17	0.49	0.84
3a	Cu-DAN	*COH-CO+ H ⁺ +e ⁻ →*C-CO + H ₂ O	H-shuttling	-0.99	0.72	-0.21	0.49	0.82
3b	Cu-DAN		surface *H transfer	-1.25	1.66	-0.39	0.49	1.86
4a	Cu-DAN	*COH-CO+ H ⁺ +e ⁻ →*COH-CHO	surface *H transfer	-0.21	0.41	-0.10	0.49	0.45
4b	Cu(100)		surface *H transfer	-0.04	0.69	-0.05	0.49	0.72
5	Cu-DAN	*COH-CHO+ H ⁺ +e ⁻ →*CHOH-CHO	surface *H transfer	-0.38	0.52	-0.08	0.49	0.56
6	Cu-DAN	*COH-CHO+ H ⁺ +e ⁻ →*C-CHO	surface *H transfer	0.04	1.02	-0.11	0.49	1.07
7	Cu-DAN	*CHOH-CHO+ H ⁺ +e ⁻ →*CH ₂ OH-CHO	surface *H transfer	-0.27	0.25	0.04	0.49	0.23
8	Cu-DAN	*CH ₂ OH-CHO+ H ⁺ +e ⁻ →*CH ₂ OH-CH ₂ O	surface *H transfer	-0.29	0.39	-0.08	0.49	0.43
9	Cu-DAN	*CH ₂ OH-CH ₂ O+ H ⁺ +e ⁻ →CH ₂ OH-CH ₃ +*O	surface *H transfer	-0.58	0.98	-0.15	0.49	1.05
10	Cu-DAN	*CH ₂ OH-CH ₂ O+ H ⁺ +e ⁻ →*CH ₂ OH-CH ₂ OH	H-shuttling	-0.19	0.73	-0.18	0.49	0.82

^a U^0 is the potential where reaction $*A+H^++e^- \rightarrow *A+*H$ possess zero free energy change i.e. $G(*A+*H) + eU^0 - G(*A) - 1/2H_2 = 0$, where *A means the system with A adsorbed on the surface.

^b β' is the reaction symmetry factor, which is approximated as 0.49 for all elementary steps.⁷

Table S9. Atomic coordinates of IS, TS, and FS of Reaction 4c listed in Table S1.

Reaction 4b: *COH-CO+ H ⁺ +e ⁻ →*COH-CHO on planar Cu (100) via surface *H transfer					
IS		TS		FS	
Cu C H O 1.00000000000000 10.903325675399996 0.000000000000000 0.000000000000000 0.000000000000000 10.903325675399996 0.000000000000000 0.000000000000000 0.000000000000000 10.634441891799999 Cu C H O 36 2 2 2 Selective dynamics Direct		Cu C H O 1.00000000000000 10.903325675399996 0.000000000000000 0.000000000000000 0.000000000000000 10.903325675399996 0.000000000000000 0.000000000000000 0.000000000000000 10.634441891799999 Cu C H O 36 2 2 2 Selective dynamics Direct		Cu C H O 1.00000000000000 10.903325675399996 0.000000000000000 0.000000000000000 0.000000000000000 10.903325675399996 0.000000000000000 0.000000000000000 0.000000000000000 10.634441891799999 Cu C H O 36 2 2 2 Selective dynamics Direct	
0.000000000000000 0.000000000000000 0.000000000000000 F F F 0.1661041259954941 0.0008695378088244 0.1619882777796406 T T T 0.9995854207921430 0.1670516348230785 0.1649245184631450 F F T 0.166666666666643 0.166666666666643 0.000000000000000 F F F 0.000000000000000 0.333333333333357 0.000000000000000 F F F 0.1664415101985676 0.333290967530651 0.161782274428833 T T T 0.9997562743553990 0.4997578192274045 0.1622764859777086 T T T 0.166666666666643 0.500000000000000 0.000000000000000 F F F 0.000000000000000 0.666666666666643 0.000000000000000 F F F 0.1639901206847034 0.6682089858481457 0.1611648800777758 T T T 0.9991196295680950 0.8338781576929283 0.1620198075772152 T T T 0.166666666666643 0.833333333333357 0.000000000000000 F F F 0.333333333333357 0.000000000000000 0.000000000000000 F F F 0.5002715303656241 0.0002944146804081 0.1623122392668561 T T T 0.3336233147562353 0.1663903303844037 0.1621524171165534 T T T 0.500000000000000 0.166666666666643 0.000000000000000 F F F 0.333333333333357 0.333333333333357 0.000000000000000 F F F 0.5025121458238192 0.3314724932912396 0.1678101234102215 T T T 0.3318164580322804 0.5016036180781258 0.1692018541826215 T T T 0.500000000000000 0.500000000000000 0.000000000000000 F F F 0.333333333333357 0.666666666666643 0.000000000000000 F F F 0.4981462177966607 0.6681366770134289 0.1692124547645107 T T T 0.3317795142791436 0.8361575700248703 0.1611647837928961 T T T 0.500000000000000 0.833333333333357 0.000000000000000 F F F 0.666666666666643 0.000000000000000 0.000000000000000 F F F 0.83329676754448812 0.0002971881994578 0.1649166396738098 T T T 0.6682781463880616 0.1644864174007575 0.1651160889588236 F T T 0.833333333333357 0.166666666666643 0.000000000000000 F F F 0.666666666666643 0.333333333333357 0.000000000000000 F F F 0.8354067672288140 0.3318334795686460 0.1649933419499269 T T T 0.6684751656146590 0.497672363318578 0.1677835236298524 T T T 0.833333333333357 0.500000000000000 0.000000000000000 F F F 0.666666666666643 0.666666666666643 0.000000000000000 F F F 0.8336068064568966 0.6664258514133563 0.1621331480542856 T T T 0.6666895664454081 0.8334454813277262 0.1617969452907017 T T T 0.833333333333357 0.833333333333357 0.000000000000000 F F F 0.4554538836332186 0.5444410637074751 0.3044095668841552 T T T 0.5514402691501205 0.4484101218772729 0.3139921071042192 T T T 0.4611097447278152 0.5393161924450083 0.483285469834224 T T T 0.8309714754755351 0.1695980991580818 0.2185727790337578 T T T 0.4146957401267218 0.5849918964564399 0.4185270683446837 T T T 0.5901722201266092 0.4102828789059565 0.4167617771546612 T T T		0.000000000000000 0.000000000000000 0.000000000000000 F F F 0.1660864284965375 0.000690524000273 0.1627564135632032 T T T 0.999828870111660 0.1668916261782245 0.1626618321231320 T T T 0.166666666676395 0.166666666676395 0.000000000000000 F F F 0.000000000000000 0.333333333123605 0.000000000000000 F F F 0.165822599191973 0.3326776229563612 0.1619516827540445 T T T 0.9997830061794007 0.4998960179630280 0.1625296523692658 T T T 0.16666666676395 0.500000000000000 0.000000000000000 F F F 0.000000000000000 0.66666666676395 0.000000000000000 F F F 0.1633564751298621 0.6681582706254641 0.1617415544105775 T T T 0.9993978075783454 0.8339086054070536 0.1627536257032900 T T T 0.16666666676395 0.833333333123605 0.000000000000000 F F F 0.333333333123605 0.000000000000000 0.000000000000000 F F F 0.5001249938557017 0.0002197588932932 0.1625404939251031 T T T 0.3328861589628708 0.1657047200658749 0.1619740438635099 T T T 0.500000000000000 0.166666666676395 0.000000000000000 F F F 0.333333333123605 0.333333333123605 0.000000000000000 F F F 0.5006357921907516 0.3309144818895444 0.1663883799392043 T T T 0.3334125651700385 0.4995335749729921 0.1678294464889087 T T T 0.500000000000000 0.500000000000000 0.000000000000000 F F F 0.333333333123605 0.66666666676395 0.000000000000000 F F F 0.5001992639966042 0.6667820022390294 0.1680663349987641 T T T 0.3318355744755442 0.8366914310170881 0.1617232703452010 T T T 0.500000000000000 0.833333333123605 0.000000000000000 F F F 0.66666666676395 0.000000000000000 0.000000000000000 F F F 0.8330999758248234 0.0003237298301323 0.1626557912014171 T T T 0.6674386438918012 0.1649206114047846 0.1634686225089745 T T T 0.833333333123605 0.16666666676395 0.000000000000000 F F F 0.66666666676395 0.333333333123605 0.000000000000000 F F F 0.835419044383710 0.3325601912296752 0.1634518135231096 T T T 0.6689797095209409 0.4993305772400200 0.166504791496560 T T T 0.833333333123605 0.500000000000000 0.000000000000000 F F F 0.66666666676395 0.66666666676395 0.000000000000000 F F F 0.8342751768706803 0.6671091429721240 0.1619770986975105 T T T 0.6673077023610385 0.8341505597131198 0.1619687885209637 T T T 0.833333333123605 0.833333333123605 0.000000000000000 F F F 0.4315929954476401 0.5676622453318021 0.3126968767666341 T T T 0.5127388659590715 0.4918038624039694 0.3746750242326554 T T T 0.3773172475163558 0.6196597526995888 0.4842695374618884 T T T 0.6272254083304288 0.3726698310489057 0.2440934425380004 T T T 0.3583034425459599 0.6391831356396294 0.3964899238392943 T T T 0.5604084871526547 0.4478124346847349 0.4646995466481276 T T T		0.000000000000000 0.000000000000000 0.000000000000000 F F F 0.1656183641702520 0.0009120206962821 0.1625777155000722 T T T 0.9996863978847994 0.1668664325953029 0.1627126800127553 T T T 0.166666667033496 0.166666667033496 0.000000000000000 F F F 0.000000000000000 0.333333332966504 0.000000000000000 F F F 0.1665743031880270 0.3303611318288907 0.1619518881803572 T T T 0.9991427312927184 0.4993331392748290 0.1625478197274055 T T T 0.166666667033496 0.500000000000000 0.000000000000000 F F F 0.000000000000000 0.666666667033496 0.000000000000000 F F F 0.1622367575357500 0.6677071395809152 0.1622162458447615 T T T 0.9991126624570652 0.8342478379066895 0.1625551841130585 T T T 0.166666667033496 0.833333332966504 0.000000000000000 F F F 0.333333332966504 0.000000000000000 0.000000000000000 F F F 0.5006544469543923 0.0008257786984203 0.1626075557627554 T T T 0.3329985705370204 0.1657798649206059 0.1628190670802992 T T T 0.500000000000000 0.166666667033496 0.000000000000000 F F F 0.333333332966504 0.333333332966504 0.000000000000000 F F F 0.5001192642486006 0.3299752870446936 0.1618319291567784 T T T 0.333453045168431 0.4990121075085339 0.1676474627907450 T T T 0.500000000000000 0.500000000000000 0.000000000000000 F F F 0.333333332966504 0.666666667033496 0.000000000000000 F F F 0.5000054676479334 0.6671354351717098 0.1680288414207116 T T T 0.3322061947958173 0.8380210143808798 0.1620445200392823 T T T 0.500000000000000 0.833333332966504 0.000000000000000 F F F 0.666666667033496 0.000000000000000 0.000000000000000 F F F 0.8331263542994207 0.0001650938241613 0.1627000399878095 T T T 0.6670816427661515 0.1661724664039810 0.1625402005455117 T T T 0.833333332966504 0.166666667033496 0.000000000000000 F F F 0.666666667033496 0.333333332966504 0.000000000000000 F F F 0.8337281909035029 0.3329582240493775 0.1625430453029703 T T T 0.6689268903690056 0.4999588078432516 0.1617648901991565 T T T 0.833333332966504 0.500000000000000 0.000000000000000 F F F 0.666666667033496 0.666666667033496 0.000000000000000 F F F 0.8341611197343570 0.6669487047425560 0.1627844198494415 T T T 0.6667821242038060 0.8332780704947425 0.1619951397918860 T T T 0.833333332966504 0.833333332966504 0.000000000000000 F F F 0.4077626903381310 0.5908809374249930 0.3109118082981768 T T T 0.4841703392037808 0.5201356331287620 0.3972210108965136 T T T 0.3444777582969926 0.650923916088790 0.466071836578153 T T T 0.5514938920491012 0.4553852715759961 0.3518780932489524 T T T 0.3274867100251982 0.6671011635961941 0.3754455049486158 T T T 0.4749276522117104 0.5311597608130554 0.5130415835288753 T T T	

Table S11. Atomic coordinates of IS, TS, and FS of Reaction 5 listed in Table S1.

Reaction 6: *COH-CHO+ H ⁺ +e ⁻ →*C-CHO on Cu-DAN via surface *H transfer									
IS			TS			FS			
Cu C H O 1.0000000000000000 12.855004805000001 0.0000000000000000 0.0000000000000000 -6.4291002405000004 11.1357880710000003 0.0000000000000000 0.0000000000000000 0.0000000000000000 15.2994003295999992			Cu C H O 1.0000000000000000 12.855004805000001 0.0000000000000000 0.0000000000000000 -6.4291002405000004 11.1357880710000003 0.0000000000000000 0.0000000000000000 0.0000000000000000 15.2994003295999992			Cu C H O 1.0000000000000000 12.855004805000001 0.0000000000000000 0.0000000000000000 -6.4291002405000004 11.1357880710000003 0.0000000000000000 0.0000000000000000 0.0000000000000000 15.2994003295999992			
Cu C H O 55 2 3 2 Selective dynamics Direct			Cu C H O 55 2 3 2 Selective dynamics Direct			Cu C H O 55 2 3 2 Selective dynamics Direct			
0.0000000000000000 0.0000000000000000 0.0000000000000000 F F F	0.0000000000000000 0.0000000000000000 0.0000000000000000 F F F	0.0000000000000000 0.0000000000000000 0.0000000000000000 F F F	0.0000000000000000 0.0000000000000000 0.0000000000000000 F F F	0.0000000000000000 0.0000000000000000 0.0000000000000000 F F F	0.0000000000000000 0.0000000000000000 0.0000000000000000 F F F	0.0000000000000000 0.0000000000000000 0.0000000000000000 F F F	0.0000000000000000 0.0000000000000000 0.0000000000000000 F F F	0.0000000000000000 0.0000000000000000 0.0000000000000000 F F F	0.0000000000000000 0.0000000000000000 0.0000000000000000 F F F

Supplementary References

- 1 T. Cheng, H. Xiao, W. A. Goddard III, *Proc. Natl. Acad. Sci. U.S.A.*, 2017, **114**, 8, 1795–1800.
- 2 Y. Lum, T. Cheng, W. A. Goddard III, J. W. Ager, *J. Am. Chem. Soc.*, 2018, **140**, 9337–9340.
- 3 F. Calle-Vallejo, M. T. M. Koper, *Angew Chem. Int. Ed.*, 2013, **52**, 28, 7282–7285.
- 4 G. Henkelman, H. J. Jónsson, *Chem. Phys.*, 2000, **113**, 9978-9985.
- 5 X. Nie, M. R. Esopi, M. J. Janik, A. Asthagiri, *Angew. Chem., Int. Ed.*, 2013, **52**, 2459–2462.
- 6 W. Luo, X. Nie, M. J. Janik, A. Asthagiri, *ACS Catal.*, 2016, **6**, 219–229.
- 7 J. A. Garza, T. A. Bell, M. Head-Gardon, *ACS Catal.*, 2018, **8**, 1490–1499.